ACS APPLIED MATERIALS & INTERFACES

Research Article

www.acsami.org

Combination of iCVD and Porous Silicon for the Development of a Controlled Drug Delivery System

Steven J. P. McInnes,[†,‡] Endre J. Szili,[‡] Sameer A. Al-Bataineh,[‡] Jingjing Xu,[§] Mahriah E. Alf,[§] Karen K. Gleason,[§] Robert D. Short,[‡] and Nicolas H. Voelcker*[,‡]

[†]School of Chemical and Physical Sciences, Flinders University, Bedford Park, SA 5042 Australia

[‡]Mawson Institute, University of South Australia, Mawson Lakes, SA 5095 Australia

[§]Department of Chemical Engineering, Massachusetts Institute of Technology, Cambridge, Massachusetts 02139, United States

Supporting Information

ABSTRACT: We describe a pH responsive drug delivery system which was fabricated using a novel approach to functionalize biodegradeable porous silicon (pSi) by initiated chemical vapor deposition (iCVD). The assembly involved first loading a model drug (camptothecin, CPT) into the pores of the pSi matrix followed by capping the pores with a thin pH responsive copolymer film of poly(methacrylic acid-co-ethylene dimethacrylate) (p(MAA-co-EDMA)) via iCVD. Release of CPT from uncoated pSi was identical in two buffers at pH 1.8 and pH 7.4. In contrast, the linear release rate of CPT from the pSi matrix with the p(MAA-co-EDMA) coating was dependent on the pH; release of CPT was more than four times faster at pH 7.4 (13.1 nmol/(cm^2 h)) than at pH 1.8 (3.0 nmol/(cm^2 h)). The key advantage of this drug delivery approach over existing ones based on pSi is that the iCVD coating can be applied to the pSi matrix after drug loading without degradation of the drug because the process does not expose the drug to harmful solvents or high temperatures and is independent of the surface chemistry and pore size of the nanoporous matrix.

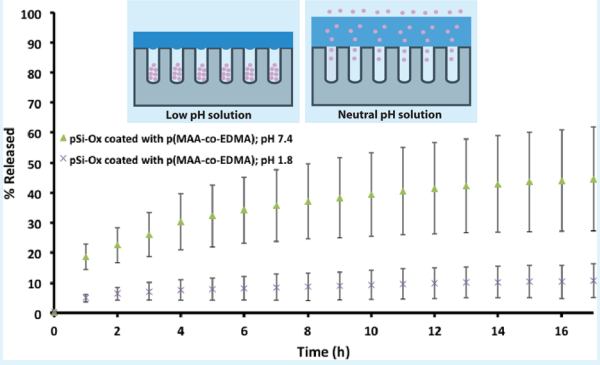

KEYWORDS: *drug release, iCVD, pH-responsive, porous silicon*

1. INTRODUCTION

Modern therapeutic human healthcare has significantly benefitted from recent developments in targeted and controlled drug delivery technologies.[1−7] Therapeutic drugs can now be made with controllable release kinetics and absorption rates thus improving both their efficacy and efficiency, and ultimately therapeutic outcomes. For the safety and convenience of the patient, drugs should be preferably delivered by noninvasive methods such as oral administration. However, in many circumstances this is not possible. For example, protein-based drugs are susceptible to enzymatic degradation and many medications that need to pass through the stomach are not stable in low pH environments. To this end, advancements in nanotechnology including the development of nanoporous drug delivery vehicles have led to significant improvements in drug delivery technologies.[8] However, improvements in current drug delivery technologies will potentially provide patients with more efficient noninvasive drug delivery methods, thereby decreasing adverse side-effects, reducing the dosing frequency and enhancing the mode of action of drugs.

In this paper, we investigate a novel approach for the fabrication of a nanocomposite drug delivery device. The bulk of the device consists of porous silicon (pSi). pSi is nontoxic and biodegradable.[9] It exhibits excellent biocompatibility when implanted in the body material (e.g., for ocular therapy)[10] and it can be used as an in situ biosensor.[11] pSi can also be effectively used for drug delivery.[8,12−14] The attractive qualities of pSi for drug delivery include a tunable drug loading capacity and biodegradability, a high surface area ratio of 100−800 m^2/g[15] for drug loading, photonic properties that are exploitable for biosensing[16−19] and for self-reporting drug delivery,[20,21] and versatility in design such as fabrication into membranes and micro- or nanoparticles,[22−27] making it suitable for multiple applications including implantation or injection. Finally, pSi degrades into silicic acid in aqueous environments, which is a nontoxic and common food additive.[28]

After fabrication of the pSi support through electrochemical etching, a model drug was loaded into the pores through adsorption. Camptothecin (CPT) was chosen as the model drug because its release could be easily monitored by fluorescence spectroscopy and we have previously shown that the drug can be successfully loaded into pSi.[13] To protect the

Received: April 10, 2012
Accepted: June 7, 2012
Published: June 21, 2012

drug from the external environment and enable its release from the pSi matrix in a controllable manner, the pore entrance needs to be blocked with a capping layer.[14] Ideally, the capping process should not degrade the drug if it has been preloaded into the porous matrix. Polymers are well-suited for this application because they can be tuned with a variety of different environmentally responsive properties. We used a novel approach to cap the pores through an initiated chemical vapor deposition (iCVD) process that was developed by Gleason et al.[29]

In the iCVD process, an initiating species and growth monomer are simultaneously introduced into a vacuum chamber equipped with filaments that heat the initiator to a sufficient temperature to generate free radicals without cracking the monomer, thus enabling full retention of functionality.[30−32] Adsorption of the monomer and subsequent polymerization, induced through the activated initiator, then proceeds on a cooled substrate. Recently, Gleason et al. have demonstrated the utility of the iCVD process for producing highly conformal coatings with a variety of chemistries and applications including drug delivery devices,[33] polymeric membrane filtration devices,[34] functionalization of carbon nanotube forests,[35] cell growth platforms[36] and covalent loading of bioactive ligands.[36,37]

Both the fabrication of pSi and the iCVD coating process is conducive to scale-up for industrial processes. The fabrication of pSi utilizes common industrial (wet-chemical) etching processes commonly employed by the semiconductor industry. iCVD ultilizes vacuum technology, also commonly employed by the semiconductor industry. The process can be easily scaled-up for manufacture on a commercial level.[30] The manufacture of pSi is not limited to films connected to a solid silicon support. pSi can be fabricated into free-standing membranes and micro/nanoparticles,[8] allowing drug delivery in the form of implantable wafers or injectable vehicles, respectively. pSi particles can be readily incorporated into flexible polymeric fibers.

pH responsive drug delivery systems based on pSi have previously been prepared through solution-based methods. Wu and Sailor[14] made a pH triggered drug release system using a solution of chitosan to cap insulin-loaded pSi. Upon switching from pH 7.4 to pH 6.0, swelling of the chitosan capping layer (2−3 μm thick) was observed and the drug release was stimulated. This system could successfully sustain the release of insulin for more than one h. In another example, Xu et al.[38] used the layer by layer assembly of poly(allylamine hydrochloride) and poly(styrene sulfonate) onto Fe_3O_4/SiO_2 composites. Their system could control the drug release for over 50 h, with the final release percentage ranging from 20 to 100%. Xue et al.[39] capped drug-loaded porous silicon nanoparticles with cyclodextrin. Their system was shown to release 100% of the loaded drug within 5 h. Finally, Gao et al.[40] produced mesoporous silica spheres grafted with pH-responsive propyldiethylenetriamine groups. These materials were able to control the release of ibuprofen, which was dependent on the amount of propyldiethylenetriamine groups and the pH of the drug release medium. To the best of our knowledge, this paper is the first report of using iCVD to cap drug-loaded pSi. This approach may be advantageous because the iCVD allows the substrate to be coated at room temperature, and therefore is ideally suited for use with drug molecules that are susceptible to degradation at elevated temperatures, such as proteins and antibodies. In addition, the solvent-free nature allows full retention of the loaded drug molecules.[33]

We used the iCVD process to cap CPT-loaded pSi with methyl methacrylate (MAA) in the presence of a cross-linking monomer, ethylene dimethacrylate (EDMA) (Scheme 1). The

Scheme 1. Fabrication of the pH responsive Nanoporous Drug Delivery Device Illustrating the Nanoporous Silicon Matrix, Loading of the Drug into the Matrix, and Finally the Capping of the Drug-Loaded Pores with the pH Responsive iCVD Film

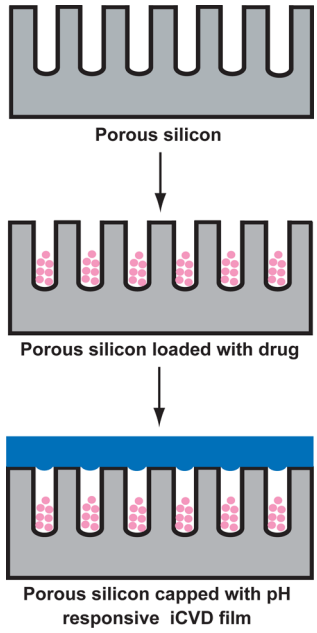

p(MAA-co-EDMA) copolymer displays a pH responsive property.[33,41] It was anticipated that at low pH, the cross-linked film will provide a protective barrier against diffusion of the drug, while at neutral pH the film will allow for diffusion of the drug out of the porous layer due to the polymer's pH-dependent swelling behavior (Scheme 2).[33,41] The release of CPT from the nanocomposite drug delivery device was investigated in buffered solutions of low and neutral pH.

Scheme 2. Release characteristics of the Drug from the Nanoporous Drug Delivery Device That Had Been Capped With a pH Responsive iCVD Film[a]

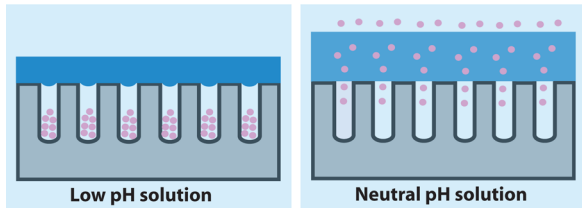

[a]In a low pH buffered solution, the film is expected to remain in a collapsed state, inhibiting the release of the drug. In contrast, in a higher (neutral) pH buffered solution, the iCVD film should swell, enabling diffusion of the drug through the polymer and into the solution.

2. EXPERIMENTAL PROCEDURES

2.1.1. Description of Chemicals. Hydrofluoric acid (HF) 48% (Merck), dichloromethane (CH_2Cl_2, Labserv, analytical grade, 99.5%), methanol (Merck, analytical grade, 99.5%), acetone (Ajax, analytical grade, 99.5%), and ethanol (Ajax, absolute, 100%) were used for etching and washing without further purification. N,N-dimethylformamide (DMF, EMD Chemicals, Belgium) was purified via standard laboratory protocols including drying over $MgSO_4$ followed by distillation at reduced pressure.[42] Conductivity water 18.2 MΩ was obtained from a Water Pro PS water purifier (Labconco). CPT (Sigma, 95%) was stored at 2−4 °C and protected from light at all times. Phosphate buffered saline (PBS) was prepared from sodium chloride (NaCl, AR, Chemsupply 99.0%, (8 g/L)), potassium chloride (KCl, AR, Biolab Scientific, 99.5%, (0.2 g/L)), disodium phosphate dihydrate ($Na_2HPO_4{\cdot}2H_2O$, AR, Chemsupply, 99.0%, (1.12 g/L)) and potassium dihydrogen orthophosphate (KH_2PO_4, AR, Ajax, 99.0%, (0.24 g/L)). The pH was adjusted to 7.4 or 1.8 with 1 M solutions of sodium hydroxide (NaOH, Ajax, analytical grade) or hydrochloric acid (HCl, Aldrich, reagent grade) in conductivity water.

2.1.2. Preparation of Oxidized pSi Films. P-type silicon wafers from Silicon Quest International (boron doped, resistivity = 3−6 Ωcm, ⟨1−0−0⟩) were etched in 1:1 HF:ethanol electrolyte at a current density of 36.67 mA/cm^2 in a poly(tetrafluoroethylene) (PTFE) cell with an exposed area of 1.8 cm^2. The pSi was then consecutively washed with copious amounts of methanol, ethanol, acetone, and CH_2Cl_2 and dried in a stream of nitrogen gas. Thermal oxidation was performed using a tube furnace (Labec, Australia) for 1 h at 400 °C.

2.1.3. Loading of the Model Drug (CPT) into pSi. pSi layers were loaded with the model drug using a solution of 2.5 mg mL^{-1} CPT in dry, distilled DMF for 2 h before being removed and dried under vacuum (10 mm of Hg) in a desiccator. This procedure was performed before the deposition of the p(MAA-co-EDMA) film. The total CPT loading for each of the materials was calculated gravimetrically on a five decimal place balance. The average amount of drug loaded into the pSi matrix was 55 nmol/cm^2. These total loading values were then used to convert the release amounts into percentages. The release amounts were calculated via the use of a calibration curve and normalized to the surface area of the material to allow for comparison of the results between different samples.

2.1.4. Initiated Chemical Vapor Deposition (iCVD). iCVD was performed in a custom-built vacuum reactor (Sharon Vacuum), as previously described.[43,44] Thermal excitation was provided by heating a nichrome filament (80:20 Ni/Cr) mounted in a parallel array to 285 °C, and the temperature was measured by a thermocouple attached to one of the filaments. The filament holder straddled the deposition stage, which was maintained at 20 °C using water cooling. The vertical distance between the filament and the stage was 2 cm. The iCVD of p(MAA-co-EDMA) was carried out using the previously optimized parameters.[33] Briefly, MAA (Aldrich, 99%) and EDMA (Aldrich, 98%) were used as the comonomers. The EDMA monomer also acted as a cross-linking agent, while tert-butyl peroxide (TBPO) (Aldrich, 97%) was the radical initiator. MAA and EDMA were heated to 70 and 100 °C, respectively, to achieve sufficient vapor flow, while TBPO was used at ambient temperature. Flow rates of MAA, EDMA and TBPO were controlled with mass flow controllers (MKS) at 0.6, 0.1, and 0.1 sccm, respectively. Total pressure in the reactor chamber was maintained at 0.5 Torr. During deposition, film growth was simultaneously monitored on a flat Si wafer in situ through laser interferometry and controlled to a thickness of 350 nm.

2.1.5. Infrared (IR) Spectroscopy. Attenuated total reflectance infrared (ATR-IR) spectra were obtained using a Nicolet Nexus 870 Fourier transform (FT) IR spectroscope (Thermo Electron Corporation, USA) using a Smart Orbit diamond accessory capable of analyzing in the range of 200−30,000 cm^{-1}. The IR spectroscope was equipped with a deuterated triglycine sulfate detector with an in-built thermo-electric cooler. Spectra of the pSi layers were recorded and analyzed using OMNIC version 7.0 software, in the range of 650−4000 cm^{-1}, at a resolution of 4 cm^{-1} and the background was taken using an unetched flat Si wafer. All IR spectra are presented in absorbance normalized to the Si−O peak at approximately 1100 cm^{-1} and scaling the entire spectra so that the Si−O peak is equal to 1 AU in every spectra.

2.1.6. Atomic Force Microscopy (AFM). Tapping mode AFM was performed on a Multimode Nanoscope with a Nanoscope IV controller (Veeco Corporation). Commercial Si cantilevers (FESP) acquired from Veeco Corporation with the following specifications were used for all experiments; beam shaped, 225 μm length, 28 μm width, 3 μm thickness, 2.8 N/m force constant, 75 kHz resonance frequency and a tip height and radius of 10−15 μm and <8 nm, respectively. All AFM imaging was performed at ambient conditions and the images were processed and analyzed using the Nanoscope 5.31r1 software (Veeco Corporation). The diameter of the pores was measured by cross-sectional analysis using the Nanoscope AFM software. The diameter of 20 pores was measured to determine the average pore diameter.

2.1.7. X-ray Photoelectron Spectroscopy (XPS). XPS was performed using an AXIS Ultra DLD spectrometer (Kratos Analytical, UK) equipped with a monochromatic Al Kα radiation source ($h\nu$ - 1486.6 eV) at a power of 225 W. The pass energy for survey spectra, recorded over the energy range 0−1000 eV, was 160 eV with 0.5 eV step size and the pass energy for high-resolution C 1s spectra was 20 eV with 0.1 eV step size. The analysis area was approximately 700 μm × 300 μm. The spectra were acquired at a takeoff angle of 90°. Elements present on the surface were identified from survey spectra and quantified in atomic percentage (at. %) with CasaXPS Software (version 2.3.14, www.casaxps.com) using a Shirley-type background and applying the relative sensitivity factors supplied by the manufacturer of the instrument. In order to minimize X-ray-induced sample degradation, the exposure time was kept to the minimum required to obtain an adequate signal-to noise ratio. Charging effect of the samples during analysis was corrected using a reference value of 285.0 eV; the binding energy of the main C 1s component arising from neutral hydrocarbon (CH_x).[45] Two nonoverlapping areas of each surface were analyzed and the standard deviation (SD) calculated.

2.1.8. Scanning Electron Microscopy (SEM). SEM was performed on a XL30 field-emission SEM (acceleration voltage of 10 kV) (Philips, Holland). To help facilitate the dissipation of charge build-up, we coated samples with platinum to a thickness of 5 nm before analysis, according to our standard laboratory protocol.[10]

2.1.9. Water Contact Angle (WCA) Measurements. WCA's were measured by placing a 1 mL drop of water on the sample surface and capturing a digital image using a Panasonic Super Dynamic wv-BP550 Closed Circuit TV camera. The contact angle measurements were analyzed by Scion Image for Windows Framegrabber software (Beta version 4.0.2).

2.1.10. Interferometric Reflectance Spectroscopy. Interferometric reflectance spectroscopy was used to monitor the effective optical thickness (EOT) of the pSi layer in time-lapse mode. The experiments were performed using a custom-built interferometer with an S2000 CCD Detector (Ocean Optics, USA). pSi substrates were placed inside a custom-built glass fluidic cell that allowed solutions to be flowed over the sample while monitoring the EOT in real time. Detailed description of the experimental setup is provided elsewhere.[46]

2.1.11. Drug Release Experiments. CPT release was monitored via fluorimetry. Fluorimetry was performed on a Perkin-Elmer Instruments LS55 luminescence spectrometer with an excitation wavelength of 340 nm and emission wavelength of 434 nm. The slit width was set to 3 nm and the photomultiplier voltage was set to 775 V. The cumulative release data of CPT into 3 mL of PBS was monitored over a period of 17 h. Release rates were calculated from the slope of the release curves, obtained after 6 h of incubation in the drug release medium (i.e., excluding the burst and transitional release sections of the release profiles). The actual amount of CPT released was calculated with reference to a calibration curve and was normalized to the surface area of the sample to give the amount of CPT released per cm^2. This allowed the CPT release data to be directly compared between each of the samples. A minimum of three release curves was averaged to produce the release curves. All release curves were plotted with error bars, which are representative of the

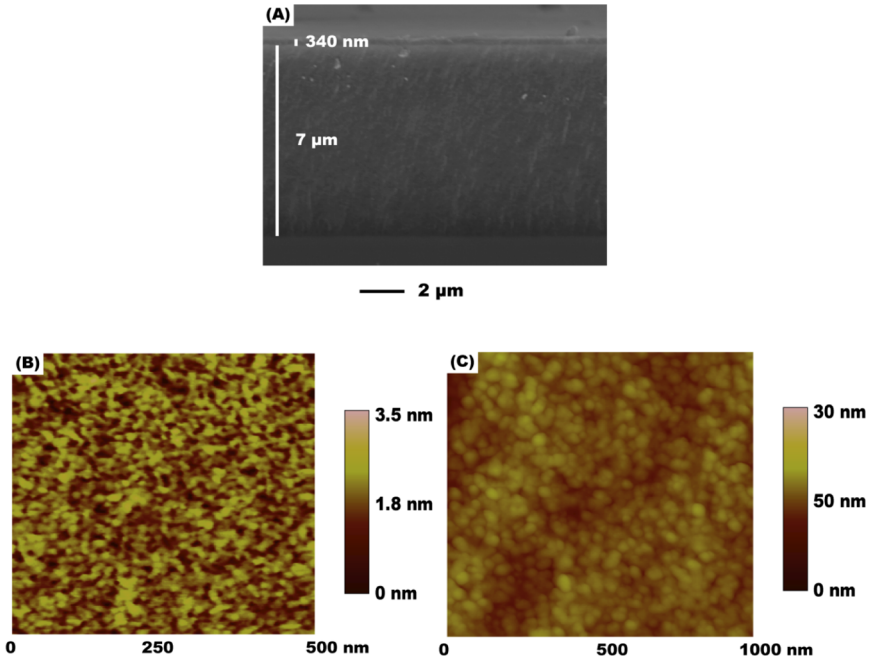

Figure 1. (A) SEM micrograph showing the cross-section of a typical p(MAA-co-EDMA) coated pSi-Ox sample, (B) an AFM image of the pSi-Ox layer (before coating with p(MAA-co-EDMA)), and (C) an AFM image of showing pore occlusion after coating pSi-Ox with p(MAA-co-EDMA). These results confirmed that the p(MAA-co-EDMA) film completely covered the pSi matrix and occluded the pores.

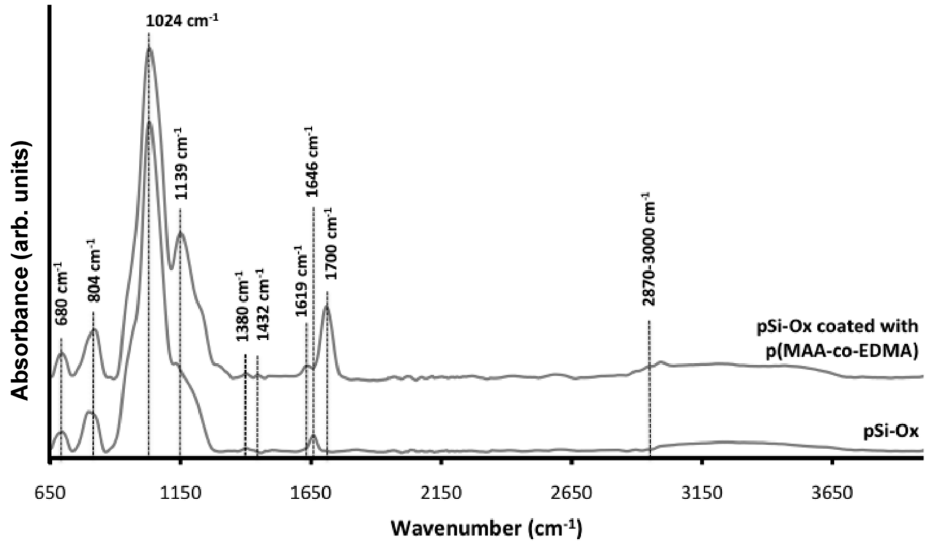

Figure 2. IR spectra of thermally oxidized pSi (pSi-Ox) and pSi-Ox coated with p(MAA-co-EDMA). This confirmed the presence of the p(MAA-co-EDMA) coating on the pSi substrates.

standard error between the averaged release runs. Release of CPT was performed in PBS at pH 7.4 and at pH 1.8. Despite the very low solubility of CPT in aqueous solutions (14.2 ± 2.9 μM)[47] sink conditions were maintained for all release experiments (maximum release concentrations were below 1.4 μM).

3. RESULTS AND DISCUSSION

3.1.1. Coating Characterization. pSi was prepared by anodization in a hydrofluoric acid (HF) and ethanol (EtOH) mixture and subsequently thermally oxidized (pSi-Ox) to render the material resistant toward corrosion in solution. Gravimetric analysis of pSi-Ox gave a porosity of approximately 75.4%. After loading pSi with CPT, the pore entrance was capped with p(MAA-co-EDMA) via an iCVD process. Cross-sectional SEM analysis of the p(MAA-co-EDMA) coated pSi-Ox surface revealed a polymer film of 340 nm covering the 7 μm deep pSi layer (Figure 1A). The surface topography of pSi-Ox before and after coating with p(MAA-co-EDMA) was analyzed by means of atomic force microscopy (AFM). Uncoated pSi-Ox had an average pore diameter of 10.1 ± 2.3 nm and a surface roughness of 0.4 nm (Figure 1B). AFM confirmed that the iCVD of p(MAA-co-EDMA) had completely occluded the pores (Figure 1C), and resulted in an increase in the surface roughness to 5.1 nm.

Chemical analysis by infrared (IR) spectroscopy confirmed the presence of the p(MAA-co-EDMA) polymer coating. Figure 2 shows a typical transmission IR spectrum of thermally oxidized pSi and pSi-Ox coated with the copolymer. The

dx.doi.org/10.1021/am300621k | ACS Appl. Mater. Interfaces 2012, 4, 3566−3574

spectrum of pSi-Ox shows a strong and broad peak centered at 1024 cm^{-1} due to asymmetric stretching vibrations of Si−O−Si surface bridging groups,[48] whereas the shoulder at 1139 cm^{-1} can be attributed to other surface oxide species.[49] The peaks at 804 cm^{-1} and 680 cm^{-1} correspond to O−Si−O bending and some residual Si−H wagging modes, respectively.[50] The spectra also contains a weak broad peak centered at approximately 3400 and 1646 cm^{-1} attributed to the presence of surface silanol groups on the oxidized pSi surface.[51] After iCVD of p(MAA-co-EDMA), the spectra still shows strong characteristic peaks for the pSi-Ox surface with additional peaks at 1380 cm^{-1} attributed to the methyl bending vibrations of p(MAA-co-EDMA), 1432 cm^{-1} assigned to the asymmetric CH_3 deformation mode and the dual peak at 2870−3000 cm^{-1} corresponding to C−H stretching vibrations of p(MAA-co-EDMA). A new peak at approximately 1700 cm^{-1} is attributed to the C═O stretching modes of p(MAA-co-EDMA), with the peak at approximately 1620 cm^{-1} attributed to vibrations of the acrylate C═C[52] probably from residual noncross-linked MAA or EDMA monomer. These spectra confirmed the presence of p(MAA-co-EDMA) on the pSi-Ox surface.

X-ray photoelectron spectroscopy (XPS) analysis of uncoated and coated pSi-Ox corroborated the findings from IR spectroscopy (Table 1). The pSi-Ox showed a near stoichiometric silicon dioxide (SiO_2) layer (32.5 at% Si: 63.1 at % O). There was also the presence of slight contamination on the surface mainly from hydrocarbon and fluorine. The fluorine contaminant was presumably the result from the use of a PTFE cell during the etching procedure. After loading oxidized pSi with CPT, the surface atomic percentage (at.%) signal for carbon increased to 5.8 at %, whereas silicon decreased to approximately 29.0 at %; attributed to the drug covering the surface causing a partial attenuation of the Si signal. The atomic percentage of oxygen remained unchanged. As expected, nitrogen from CPT could not be detected on the pSi surface due to the low nitrogen content in the drug. After the iCVD coating of CPT-loaded pSi-Ox, oxygen and silicon decreased to 22.6 and 2.8 at %, respectively, whereas carbon increased to 74.6 at %. This indicated that a layer of p(MAA-co-EDMA) had been deposited over the pSi surface. Since the SEM analysis showed a 340 nm thick film, the residual silicon signal within the information depth of XPS is attributed to silicon particles deposited on the sample during the cutting of the sample required for XPS analysis. The presence of pinholes in the coating is unlikely given that the coating thickness exceeds several hundreds of nm and that the SEM/AFM analysis of the p(MAA-co-EDMA)-coated pSi-Ox samples in images (A) and (C) in Figure 1 did not reveal any physical defects. Experimentally, we observed an O/C ratio of 0.30 for p(MAA-co-EDMA), which is close to the expected theoretical value of 0.36.

Table 1. Summary of the XPS results for pSi-Ox and pSi-Ox Loaded with CPT before and after Coating with p(MAA-co-EDMA) (at. % ± SD) (n = 3)[a]

surface	C (at %)	O (at %)	F (at %)	Si (at %)
pSi-Ox	2.3 ± 1.0	63.1 ± 0.8	2.1 ± 0.1	32.5 ± 0.1
pSi-Ox loaded with CPT	5.8 ± 0.6	63.0 ± 0.7	2.45 ± 0.5	28.8 ± 0.2
pSi-Ox loaded with CPT and coated with p(MAA-co-EDMA)	74.5 ± 0.8	22.6 ± 0.1	0.1 ± 0.1	2.8 ± 1.0

[a]These are close to the theoretical values expected for the surfaces of each modification step.

The high-resolution XPS C 1s spectrum of pSi-Ox coated with p(MAA-co-EDMA) is shown in Figure 3. The spectrum was fitted with four components corresponding to C−C/C−H (57.8%), COO/COOR (17.8%), C−O (6.5%) and C−COO (17.8%), respectively, and was comparable to that reported by Lau and Gleason for p(MAA-co-EDMA), deposited directly on silicon substrates.[33] The surface chemistry of the p(MAA-co-EDMA) coated pSi-Ox samples, as determined by IR spectroscopy and XPS analysis, remained unchanged (data not shown) after 20 h of incubation in PBS (pH 7.4) at 37 °C, indicating that the coating is not affected under the conditions used for drug release.

The wetting behavior of the p(MAA-co-EDMA) coated pSi-Ox samples was also investigated. Both the polymer film and silicon pores need to be easily wetted by the surrounding aqueous medium in order to maintain an accurate pH responsive drug release property. Flat silicon and pSi-Ox are

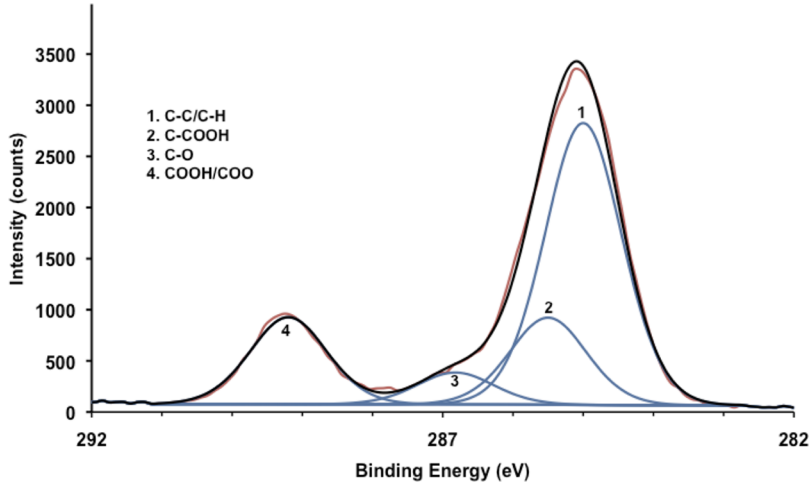

Figure 3. High-resolution C 1s XPS spectrum of pSi-Ox coated with p(MAA-co-EDMA). Black = experimental data, blue = component fitting 1−4, and red = curve fitting match to experimental data. The high-resolution spectra confirmed the presence of pMAA-co-EDMA film.

very hydrophilic with a static water contact angle (WCA) of 14 ± 1° and 10 ± 2°, respectively (Table 2). The lower WCA of pSi can be explained by the Wenzel model relating the WCA of a rough surface to a smooth surface.[53] After coating p(MAA-co-EDMA) onto flat and pSi-Ox, the WCA increased to 53 ± 2° and 57 ± 2°, respectively, due to the moderately hydrophilic chemical nature of the polymer. This result suggests that the p(MAA-co-EDMA) coated pSi can be readily wetted by water.

Table 2. WCA Measurements of Flat Si and Oxidized pSi, before and after Coating with p(MAA-co-EDMA) by iCVD (n =6)[a]

material	WCA (deg ± SD)
flat Si	14 ± 1
p(MAA-co-EDMA)-coated flat silicon	53 ± 2
pSi-Ox	10 ± 2
p(MAA-co-EDMA)-coated pSi-Ox	57 ± 2

[a]The results indicate that p(MAA-co-EDMA) coated pSi-Ox can be readily wetted, which is an important requirement of the drug delivery device.

Typically, the degradation of pSi-Ox in aqueous solution increases with pH due to hydrolysis of nonoxidized silicon hydrides.[54] Interferometric reflectance spectroscopy is commonly used to measure small changes in the thickness of the pSi films, which cannot be measured by AFM or SEM.[10,55] Using interferometric reflectance spectroscopy to measure the effective optical thickness (EOT) of the film, it was confirmed that pSi-Ox was stable at pH 1.8 over a period of 15 h, but showed significant degradation after 6 h of incubation in a buffered solution of pH 7.4 (Figure 4). In contrast, the p(MAA-co-EDMA) coating rendered the pSi-Ox matrix stable to dissolution over the same period of time in both pH 1.8 and 7.4 buffers (Figure 4). Therefore, the p(MAA-co-EDMA) coating provided a protective barrier for preventing the possibility of rapid pSi degradation in aqueous environments.

3.1.2. Drug Release. When comparing the release of drugs from these materials to a release model, a range of physical characteristics need to be taken into consideration. These include water diffusion into the matrix, drug diffusion out of the matrix, polymer swelling, polymer dissolution, pSi dissolution, porosity, and changing matrix dimensions. The experimental release data were fitted to common release models applicable to materials similar to those tested in this study and included the zero-order, first-order, Higuchi, Hixson–Crowell, and Ritger–Peppas models.[56–62]

Figure 5 shows the release profile of CPT from drug-loaded pSi-Ox at pH 1.8 and 7.4. It can be seen that drug release from uncoated pSi-Ox was almost identical at both pH conditions. In contrast, two significantly different drug release profiles were observed from CPT loaded pSi-Ox that was coated with p(MAA-co-EDMA). After 17 h of incubation in solution, only 10.7% of the drug was released at pH 1.8, whereas 44.5% of the drug was released at pH 7.4 for the same time period. The Higuchi plot (see the Supporting Information) shows a linear drug release profile excluding the initial h of burst release (time$^{1/2}$ = 1), with R^2 values of 0.993 and 0.990 for pSi-Ox and pSi-Ox coated with p(MAA-co-EDMA) at pH 7.4 and 0.983 and 0.997 for pSi-Ox and pSi-Ox coated with p(MAA-co-EDMA) at pH 1.8. This indicates that the release of CPT was mainly dependent on the diffusion of the drug through the pSi-polymer matrix and not as a result of the corrosion of the pSi-Ox matrix.

The burst and linear release rates of CPT from pSi-Ox and pSi-Ox coated with p(MAA-co-EDMA) at pH 1.8 and 7.4 and their corresponding R^2 values are shown in Table 3. The CPT release profiles from pSi-Ox were similar during the initial burst and linear release times for both pH solutions. The burst release rate of CPT from p(MAA-co-EDMA)-coated pSi-Ox at pH 7.4 was approximately half of that observed from uncoated pSi-Ox. At pH 1.8, the burst and linear release rate of CPT from pSi-Ox coated with p(MAA-co-EDMA), was significantly slower at 2.75 nmol/(cm^2 h) and 0.12 nmol/(cm^2 h), respectively. These data indicate that the p(MAA-co-EDMA) coating enabled the release of CPT from the pSi-Ox matrix in a pH-dependent and controllable manner.

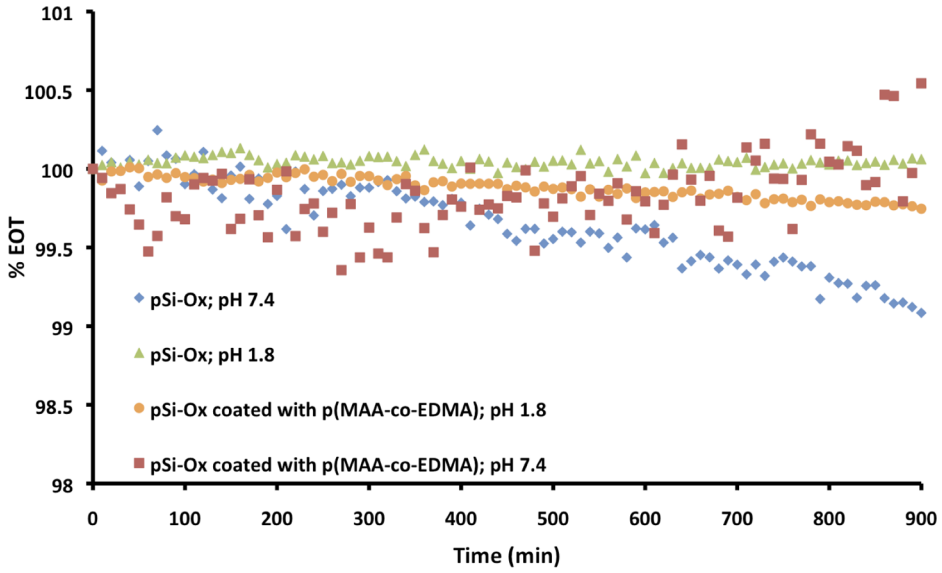

Figure 4. Effective optical thickness (EOT) measurements for pSi-Ox and pSi-Ox coated with p(MMA-co-EDMA) at pH 1.8 and 7.4, respectively (n = 3). These results indicate that the p(MAA-coEDMA) coating significantly enhanced the stability of pSi in solution. Error bars are not shown to maintain clarity of the curves; however, the error bars were not more than ±10% of the experimentally obtained data.

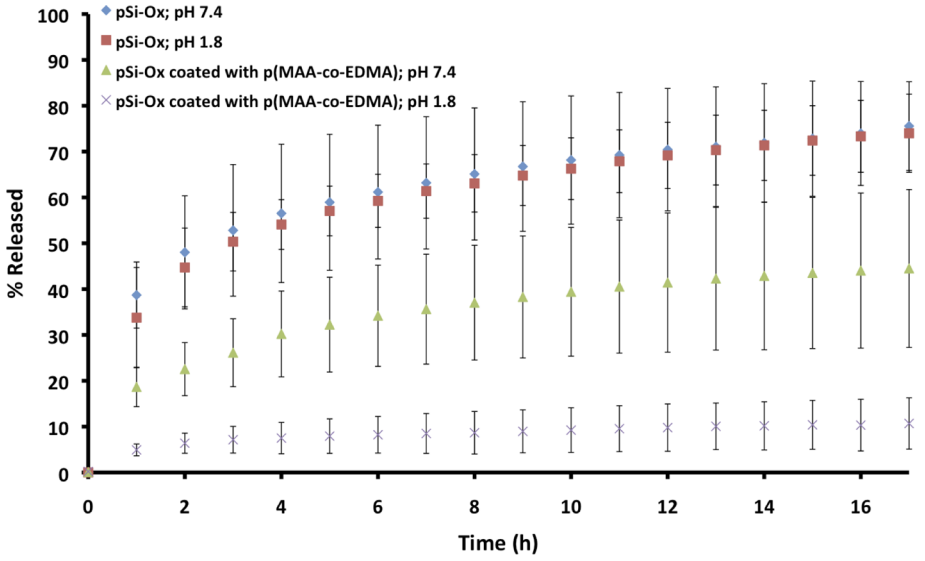

Figure 5. Drug release curves for CPT from uncoated oxidized pSi (pSi-Ox) and after coating with p(MAA-co-EDMA) at a pH of 1.8 and 7.4, respectively ($n \geq 3$). The p(MAA-co-EDMA) coating enabled the controlled pH-dependent release of the drug from the drug delivery system.

Table 3. Comparison of CPT Release Rates for the Different Drug Delivery Systems[a]

material	burst rate	burst release (%)	linear rate	linear release (%)	linearity (R^2)	final release (%)
pSi-Ox pH; 7.4[b]	21.46	21.5	0.80	20.0	0.966	74.0
pSi-Ox pH; 1.8[b]	18.88	18.9	0.76	19.0	0.982	73.3
pSi-Ox coated with p(MAA-co-EDMA); pH 7.4[b]	10.43	10.4	0.52	13.1	0.970	44.0
pSi-Ox coated with p(MAA-co-EDMA); pH 1.8[b]	2.75	2.8	0.12	3.0	0.981	10.3

[a]At pH 1.8, a minimal amount of the drug was released from the p(MAA-co-EDMA) coated pSi-Ox drug delivery device; whereas at pH 7.4 the drug was released in a controllable and linear fashion. [b]Burst release was calculated over the first 2 h. Linear release rates and R^2 values were calculated after 6 h of incubation in the drug release medium. Release rates have units of nmol/(cm^2 h).

Finally, we applied different theoretical release models (see the Supporting Information) to the drug release data (Table 4).

Table 4. Comparison of R^2 Values for Each Drug Delivery Model (entire drug delivery run) for the Different Drug Delivery Systems[a]

material	zero order	first order	Higuchi	Hixson–Crowell	Ritger–Peppas	n
pSi-Ox; pH 7.4	0.645	0.840	0.863	0.334	**0.991**	0.26
pSi-Ox; pH 1.8	0.688	0.866	0.895	0.361	**0.982**	0.31
pSi-Ox coated with p(MAA-co-EDMA); pH 7.4	0.768	0.840	0.945	0.452	**0.991**	0.31
pSi-Ox coated with p(MAA-co-EDMA); pH 1.8	0.721	0.737	0.913	0.453	**0.990**	0.27

[a]The Higuhi model was found to be the most appropriate to describe the drug release kinetics from the p(MAA-co-EDMA)-coated pSi-Ox drug delivery device.

The Ritger–Peppas model showed that the n values were all below 0.5, indicating that CPT was released according to Fickian diffusion.[63,64] Hence, we deemed the Higuchi model to be the best model to represent the drug release kinetics for all of the materials. The low n values can be explained by the nonswellable pSi-Ox matrix being much thicker (several micrometers) compared to the relatively thin (340 nm) p(MAA-co-EDMA) covering polymer film. When using the Ritger–Peppas equation, n values of less than 0.5 are only possible when porous systems are involved. In these cases, the release mechanism is a combination of diffusion through the swollen polymer and diffusion through the water-filled pores of the porous matrix.[64]

The pSi-p(MAA-co-EDMA) system used in this study could sustain the release of the drug for a longer period of time compared to other pH-dependent pSi drug delivery systems.[14,33,41] This is attributed to differences in the hydrophobicities in the drugs, type and thicknesses of the capping layers, and the surface area/volume ratios of the drug delivery devices that were used in each of these separate studies.

4. CONCLUSIONS

A pH-responsive drug delivery system was developed by coating ozone-oxidized, CPT-loaded pSi with p(MAA-co-EDMA) using an iCVD process. The effectiveness of the system was evaluated by comparing the release of CPT in acidic and neutral pH environments. Uncoated ozone-oxidized pSi showed similar drug release profiles at pH 1.8 and pH 7.4. In comparison, p(MAA-co-EDMA) coated pSi displayed a pH responsive property with a significantly slower release of the drug at pH 1.8 (0.12 nmol/(cm^2·h)) compared to pH 7.4 (0.52 nmol/(cm^2 h)) and a significant higher quantity of the drug released in a controllable, linear fashion at pH 7.4 (13.1% of the original payload over 10 h) then at pH 1.8 (3.0% of the original payload over the same time frame). This novel strategy of preparing drug delivery devices may enable site-specific targeting for drug therapy, better protection of therapeutic agents in vivo and highly tuned drug release properties.

■ ASSOCIATED CONTENT

Supporting Information

More details about the drug delivery modeling procedure and the Higuchi plots. This material is available free of charge via the Internet at http://pubs.acs.org.

■ AUTHOR INFORMATION

Corresponding Author

*E-mail: nico.voelcker@unisa.edu.au.

Notes

The authors declare no competing financial interest.

■ ACKNOWLEDGMENTS

This work was partially supported from the Australian International Science Linkage Project CG120119 and the South Australian Premier's Science Research Fund.

■ REFERENCES

(1) Andreadis, S.; Geer, D. *Trends Biotechnol.* **2006**, *24*, 331−337.
(2) Castro, G.; Panilaitis, B.; Kaplan, D. *Bioresour. Technol.* **2008**, *99*, 4566−4571.
(3) Elvira, C.; Gallardo, A.; San Roman, J.; Cifuentes, A. *Molecules* **2005**, *10*, 114−125.
(4) Sharma, S.; Jasper Nijdam, A.; Sinha, P.; Walczak, R.; Liu, X.; Cheng, M.; Ferrari, M. *Expert Opin. Drug Deliv.* **2006**, *3*, 379−394.
(5) Soppimath, K.; Aminabhavi, T.; Kulkarni, A.; Rudzinski, W. *J. Controlled Release* **2001**, *70*, 1−20.
(6) Wood, K.; Boedicker, J.; Lynn, D.; Hammond, P. *Langmuir* **2005**, *21*, 1603−1609.
(7) Tsukagoshi, T.; Kondo, Y.; Yoshino, N. *Colloids Surf., B* **2007**, *57*, 219−225.
(8) McInnes, S. J. P.; Voelcker, N. H. *Future Med. Chem.* **2009**, *1*, 1051−1074.
(9) Low, S.; Williams, K.; Canham, L.; Voelcker, N. *Biomaterials* **2006**, *27*, 4538−4546.
(10) Low, S. P.; Voelcker, N. H.; Canham, L. T.; Williams, K. A. *Biomaterials* **2009**, *30*, 2873−2880.
(11) Jane, A.; Dronov, R.; Hodges, A.; Voelcker, N. H. *Trends Biotechnol.* **2009**, *27*, 230−239.
(12) McInnes, S. J. P.; Irani, Y.; Williams, K. A.; Voelcker, N. H. *Nanomedicine* **2012**, DOI: 10.2217/NNM.11.176.
(13) Vasani, R. B.; McInnes, S. J. P.; Cole, M. A.; Jani, A. M. M.; Ellis, A. V.; Voelcker, N. H. *Langmuir* **2011**, *27*, 7843−7853.
(14) Wu, J.; Sailor, M. J. *Adv. Funct. Mater.* **2009**, *19*, 733−741.
(15) Loni, A. In *Properties of Porous Silicon*; Canham, L., Ed; Short Run Press: London, 1997.
(16) Worsfold, O.; Voelcker, N.; Nishiya, T. *Langmuir* **2006**, *22*, 7078−7083.
(17) Alvarez, S.; Derfus, A.; Schwartz, M.; Bhatia, S.; Sailor, M. *Biomaterials* **2009**, *30*, 26−34.
(18) Coffer, J.; Montchamp, J.-L.; Aimone, J.; Weis, R. *Phys. Status Solidi A* **2003**, *197*, 336−339.
(19) Palestino, G.; Agarwal, V.; Aulombard, R.; Perez, E.; Gergely, C. *Langmuir* **2008**, *24*, 13765−13771.
(20) Anglin, E.; Cheng, L.; Freeman, W.; Sailor, M. *Adv. Drug Delivery Rev.* **2008**, *60*, 1266−1277.
(21) Koh, Y.; Jang, S.; Kim, J.; Kim, S.; Ko, Y.; Cho, S.; Sohn, H. *Colloids Surf., A* **2008**, *313−314*, 328−331.
(22) Salonen, J.; Laitinen, L.; Kaukonen, A.; Tuura, J.; Bjorkqvist, M.; Heikkila, T.; Vaha-Heikkila, K.; Hirvonen, J.; Lehto, V.-P. *J. Controlled Release* **2005**, *108*, 362−374.
(23) Salonen, J.; Paski, J.; Vaha-Heikkila, K.; Heikkila, T.; Bjorkqvist, M.; Lehto, V.-P. *Phys. Status Solidi A* **2005**, *202*, 1629−1633.
(24) Lehto, V.-P.; Vähä-Heikkilä, K.; Paski, J.; Salonen, J. *J. Therm. Anal. Calorim.* **2005**, *80*, 393−397.
(25) McInnes, S.; Graney, S.; Khung, Y.-L.; Voelcker, N. *Proc. SPIE 6036* **2006**, 445−454.
(26) Meade, S.; Sailor, M. *Phys. Status Solidi RRL* **2007**, *1*, R71−R73.
(27) Wu, E.; Park, J.-H.; Park, J.; Segal, E.; Cunin, F.; Sailor, M. *ACS Nano* **2008**, *2*, 2401−2409.
(28) Canham, L.; Reeves, C.; King, D.; Branfield, P.; Crabb, J.; Ward, M. *Adv. Mater.* **1996**, *8*, 850−852.
(29) Alf, M. E.; Asatekin, A.; Barr, M. C.; Baxamusa, S. H.; Chelawat, H.; Ozaydin-Ince, G.; Petruczok, C. D.; Sreenivasan, R.; Tenhaeff, W. E.; Trujillo, N. J.; Vaddiraju, S.; Xu, J.; Gleason, K. K. *Adv. Mater.* **2009**, *21*, 1−35.
(30) Tenhaeff, W. E.; Gleason, K. K. *Adv. Funct. Mater.* **2008**, *18*, 979−992.
(31) Baxamusa, S. H.; Im, S. G.; Gleason, K. K. *Phys. Chem. Chem. Phys.* **2009**, *11*, 5227−5240.
(32) Asatekin, A.; Barr, M. C.; Baxamusa, S. H.; Lau, K. K. S.; Tenhaeff, W. E.; Xu, J.; Gleason, K. K. *Mater. Today* **2010**, *13*, 24−31.
(33) Lau, K. K. S.; Gleason, K. K. *Macromol. Biosci.* **2007**, *7*, 429−434.
(34) Gupta, M.; Kapur, V.; Pinkerton, N. M.; Gleason, K. K. *Chem. Mater.* **2008**, *20*, 1646−1651.
(35) Lau, K. K. S.; Bico, J.; Teo, K. B. K.; Chhowalla, M.; Amaratunga, G. J.; Milne, W. I.; McKinley, G. H.; Gleason, K. K. *Nano Lett.* **2003**, *3*, 1701−1705.
(36) Marí-Buyé, N.; O'Shaughnessy, S.; Colominas, C.; Semino, C. E.; Gleason, K. K.; Borrós, S. *Adv. Funct. Mater.* **2009**, *19*, 1276−1286.
(37) O'Shaughnessy, W. S.; Marí-Buyé, N.; Borrós, S.; Gleason, K. K. *Macromol. Rapid Commun.* **2007**, *28*, 1877−1882.
(38) Xu, R.; Sun, G.; Li, Q.; Wang, E.; Gu, J. *Solid State Sci.* **2010**, *12*, 1720−1725.
(39) Xue, M.; Zhong, X.; Shaposhnik, Z.; Qu, Y.; Tamanoi, F.; Duan, X.; Zink, J. I. *J. Am. Chem. Soc.* **2011**, *133*, 8798−8801.
(40) Gao, Q.; Xu, Y.; Wu, D.; Shen, W.; Deng, F. *Langmuir* **2010**, *26*, 17133−17138.
(41) Lau, K. K. S.; Gleason, K. K. *Surf. Coat. Technol.* **2007**, *201*, 9189−9194.
(42) Armarego, W.; Perrin, D. In *Purification of Laboratory Chemicals*; fourth ed.; Butterworth-Heinemann: Oxford, U.K., 1996.
(43) Lau, K. K. S.; Gleason, K. K. *Macromolecules* **2006**, *39*, 3688−3694.
(44) Chan, K.; Gleason, K. K. *Chem. Vap. Deposition* **2005**, *11*, 437−443.
(45) Beamson, G.; Briggs, D. In *High-Resolution XPS of Organic Polymers*; John Wiley and Sons: Chichester, U.K., 1992.
(46) Szili, E. J.; Jane, A.; Low, S. P.; Sweetman, M.; Macardle, P.; Kumar, S.; Smart, R. S. C.; Voelcker, N. H. *Sens. Actuators, B* **2011**, *160*, 341−348.
(47) Sætern, A. M.; Nguyen, N. B.; Bauer-Brandl, A.; Brandl, M. *Int. J. Pharm.* **2004**, *284*, 61−68.
(48) Mirji, S. A.; Halligudi, S. B.; Mathew, N.; Ravia, V.; Jacob, N. E.; Patil, K. R. *Colloids Surf., A* **2006**, *287*, 51−58.
(49) Sam, S.; Touahir, L.; Andresa, J. S.; Allongue, P.; Chazalviel, J.-N.; Gouget-Laemmel, A. C.; Villeneuve, C. H. d.; Moraillon, A.; Ozanam, F.; Gabouze, N.; Djebbar, S. *Langmuir* **2010**, *26*, 809−814.
(50) Bisi, O.; Ossicini, S.; Pavesi, L. *Surf. Sci. Rep.* **2000**, *38*, 1−126.
(51) Tommasi, E. D.; Stefano, L. D.; Rea, I.; Sarno, V. D.; Rotiroti, L.; Arcari, P.; Lamberti, A.; Sanges, C.; Rendina, I. *Sensors* **2008**, *8*, 6549−6556.
(52) Tarducci, C.; Schofield, W. C. E.; Badyal, J. P. S.; Brewer, S. A.; Willis, C. *Macromolecules* **2002**, *35*, 8724−8727.
(53) Wenzel, R. N. *Ind. Eng. Chem.* **1936**, *28*, 988−994.
(54) Szili, E. J.; Jane, A.; Low, S. P.; Sweetman, M.; Macardle, P.; Kumar, S.; Smart, R. S. C.; Voelcker, N. H. *Sens. Actuators, B* **2011**, *160*, 341−348.
(55) McInnes, S. J. P.; Thissen, H.; Choudhury, N.; Voelcker, N. *J. Colloid Interface Sci.* **2009**, *332*, 336−344.
(56) Basak, S. C.; Kumar, K. S.; Ramalingam, M. *Braz. J. Pharm. Sci.* **2008**, *44*, 488−483.

(57) Bhattacharyya, S.; Ray, S.; Gupta, B. K.; Ghosh, L. K. *Lat. Am. J. Pharm.* **2007**, *26*, 852−858.
(58) Dave, B. S.; Amin, A. F.; Patel, M. M. *AAPS PharmSciTech.* **2004**, *5*, 77−82.
(59) Naeem, M.; Mahmood, A.; Khan, S.; Shahiq, Z. *Trop. J. Pharm. Res.* **2010**, *9*, 347−354.
(60) Nie, S.; Hsiao, W. W.; Pan, W.; Yang, Z. *Int. J. Nanomed.* **2011**, *6*, 151−166.
(61) Poovi, G.; lekshmi, U. D.; Narayanan, N.; Reedy, P. *Res. J. Nanosci. Nanotechnol.* **2010**, 2−13.
(62) Ravi, P. R.; Ganga, S.; Saha, R. N. *AAPS PharmSciTech.* **2007**, *8*, 167−175.
(63) Ritger, P. L.; Peppas, N. A. *J. Controlled Release* **1987**, *5*, 37−42.
(64) Peppas, N. A. *Pharm. Acta Helv.* **1985**, *60*, 110−111.